9-2008

Percolating Oxide Film Growth During Cu(111) Oxidation

David M. Gallagher
Cedarville University, gallaghd@cedarville.edu

Percolating oxide film growth during Cu(111) oxidation

Guangwen Zhou,[1,a)] Xidong Chen,[2,3] David Gallagher,[4] and Judith C. Yang[5]

[1]*Department of Mechanical Engineering and Multidisciplinary Program in Materials Science and Engineering, State University of New York, Binghamton, New York 13902, USA*
[2]*Department of Science and Mathematics, Cedarville University, Cedarville, Ohio 45314, USA*
[3]*Materials Science Division, Argonne National Laboratory, Argonne, Illinois 60439, USA*
[4]*Department of Engineering and Computer Science, Cedarville University, Cedarville, Ohio 45314, USA*
[5]*Department of Mechanical Engineering and Materials Science, University of Pittsburgh, Pittsburgh, Pennsylvania 15261, USA*

We report *in situ* transmission electron microscopy dynamic observations of the early stage oxidation of Cu(111) surfaces at $\sim$450 °C, which show that the Cu_2O film morphology evolves with continued oxidation from initially ramified islands to irregularly connected clusters. The geometrical features of these noncompact oxide films are analyzed in terms of the scaling theory of percolation. We show by kinetic Monte Carlo simulations that the percolating oxide film growth is related to a mechanism of neighbor-dependent site percolation. © *2008 American Institute of Physics*. [DOI: 10.1063/1.2990624]

Understanding the microscopic processes controlling oxidation of metal surfaces has practical importance in many fields including environmental stability, corrosion, electrochemistry, gas sensing, heterogeneous catalysis, and dielectric film synthesis. Growth of oxide layers has been observed on many metallic systems, and models have been proposed based on the transport of ionic species through a thick and continuous oxide film.[1–4] However, such previous studies have not examined the earliest stages of oxidation beginning with island nucleation and growth, largely due to the inability of traditional techniques to perform *in situ* measurements of the structure and kinetics at the nanoscale as the reaction progresses. *In situ* ultrahigh vacuum (UHV) environmental transmission electron microscopy (TEM) provides a unique window into understanding the mechanism of nanoscale oxidation because of its capabilities for time-resolved imaging and diffraction, as well as the UHV environment necessary for atomically clean surfaces.[5–7] Here we report *in situ* UHV-TEM dynamic observations of the nanoscale oxidation of Cu(111) surfaces, which reveal the evolution of the oxide film morphology from initially ramified islands to irregularly connected oxide clusters. The growth morphology of such discontinuous, noncompact oxide films cannot be addressed by thermodynamics, i.e., the interplay between surface/interface energies and relaxation of the elastic energy due to the metal-oxide lattice mismatch, as adopted in the epitaxial growth of three-dimensional (3D) compact oxide islands.[8–10] In contrast, we show by both scaling analysis of the geometrical features of these oxide films and kinetic Monte Carlo (KMC) simulations of the oxide film growth that the noncompact morphologies of these discontinuous oxide films are of kinetic origin.

Our experiments were carried out in a modified JEOL 200CX TEM equipped to allow observation of oxidation under controlled gas environments.[11] An UHV chamber is attached to the middle of the TEM column, where the base pressure is $\sim 10^{-8}$ Torr. The microscope was operated at 100 keV to minimize the possibility of irradiation induced effects. Cu(111) single crystal films were grown on irradiated NaCl(111) by sputter deposition. The Cu films were removed from the substrate by floatation in de-ionized water, washed and mounted on a specially prepared TEM specimen holder that allows for resistive heating of the specimen up to 1000 °C. Any native Cu oxide is removed by annealing the films in the TEM under vacuum conditions at $\sim$750 °C,[12] resulting in clean copper surfaces. Oxygen gas can be admitted into the microscope through the leak valve at a partial pressure (pO_2) between 5×10^{-5} and 760 Torr. Real time observations of oxidation can be made at pressures of $\leq 5 \times 10^{-4}$ Torr.

Figure 1 shows representative images from *in situ* TEM observations of the morphological evolution of the oxide
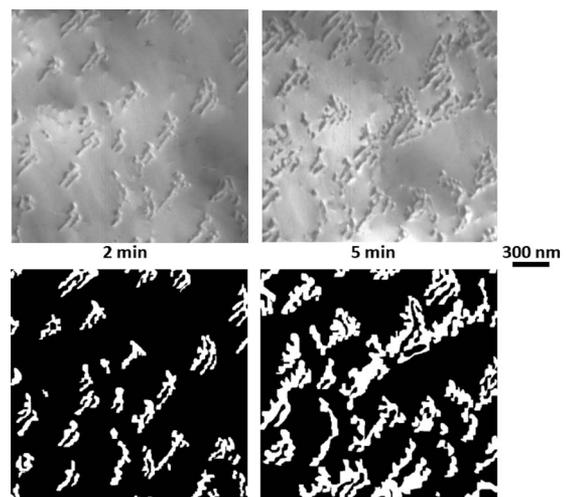

FIG. 1. *In situ* TEM images of the oxide islands formed from the oxidation of a Cu(111) surface at 450 °C and an oxygen pressure of $pO_2 = 5 \times 10^{-4}$ Torr (upper panel) and the corresponding white and black matrices (white=occupied, black=unoccupied). The images are 1024×1024 lattice units (lower panel).

---

a)Author to whom correspondence should be addressed. Electronic mail: gzhou@binghamton.edu.
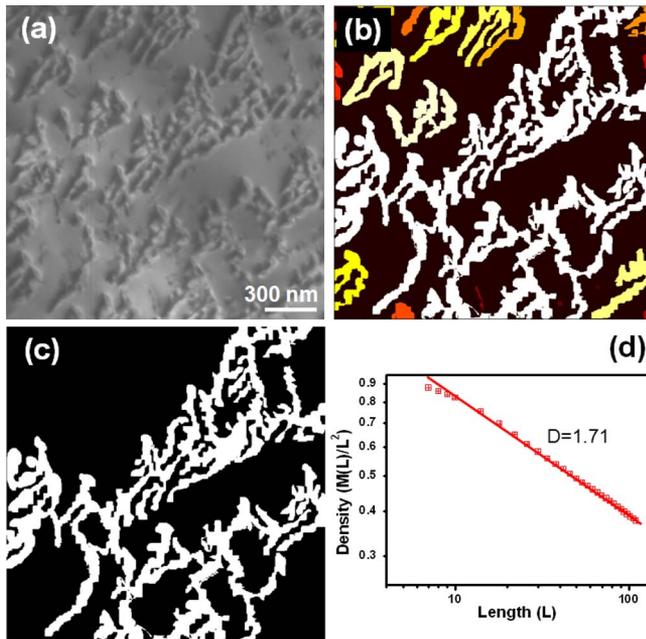
FIG. 2. (Color online) The oxide film at the percolation threshold. (a) Identification of oxide clusters by a connectivity analysis of the discontinuous oxide film. Different clusters are shown by different colors and the largest one (infinite cluster) has the brightest contrast and spans over the whole image. (b) The infinite cluster singled out from (a). (c) Scaling analysis of the infinite cluster. (d) Log-log plot of $M(L)/L^2$ vs L for the infinite cluster. The fraction dimension D for the infinite cluster is determined to be 1.71. Note that L is the number of pixels of the image and can be converted to length scale by $L(\text{nm}) = L(\text{pixel number}) \times [\text{image size(nm)}/1024]$.
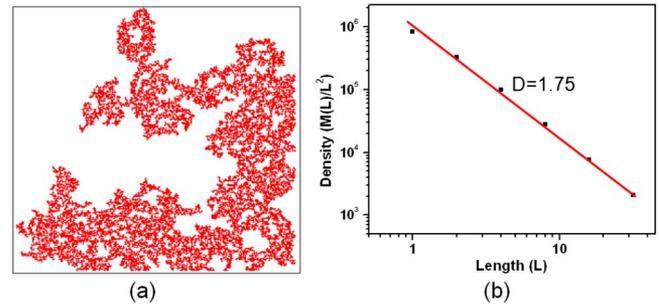

FIG. 3. (Color online) (a) The infinite cluster formed at the percolation threshold from the KMC simulations based on the neighbor-dependent site occupation mechanism. (b) Log-log plot of $M(L)/L^2$ vs L for the infinite cluster. The fraction dimension D for the infinite cluster is determined to be 1.75 (L is the number of pixels).

$$M(L) = L^D f(L/\xi) \rightarrow \begin{cases} L^D & \text{for } L \ll \xi \\ L^E & \text{for } L \gg \xi \end{cases}. \tag{1}$$

film during the oxidation of Cu(111) at 450 °C under $p\text{O}_2$ $= 5 \times 10^{-4}$ Torr. When oxygen is introduced, Cu_2O islands nucleate rapidly and form a "discontinuous-branched" shape. Further oxidation results in growth of these Cu_2O islands where they coalesce to create irregularly connected oxide clusters. Figure 1 reveals that these oxide islands have ramified morphologies and grow into each other and form a percolating network as the oxidation progresses. These discontinuous, noncompact oxide films are irregularly shaped. They look like tree branches with stringy boundaries and certainly are not describable in terms of the familiar Euclidean shapes. In order to quantitatively understand the features of the growth morphologies of the oxide films, the TEM images are digitized to a binary contrast with 1 and 0 for occupied (white) and vacant (black) sites, respectively, as shown in the lower-panel images in Fig. 1. This allows us to analyze the TEM images as a site-percolation problem.

With use of a connectivity-checking algorithm,[13] the individual Cu_2O clusters can be isolated for statistical analysis, as shown in Figs. 2(a) and 2(b). The largest cluster connecting all sides of the image is the infinite (spanning) cluster. We have found the threshold oxide coverage of 45% for the formation of the infinite cluster. The finite clusters are first eliminated leaving the infinite cluster alone [Fig. 2(c)]. Under the scaling hypothesis, the infinite cluster at the percolation threshold p_c has the property of statistical self-similarity, which can be checked by measuring the mass $M(L)$ of the infinite cluster and that of the backbone with different length scale L. At the percolation threshold, $p = p_c$, the mass of the spanning cluster scales with L as[14,15]

Here ξ is the correlation length defined as the average root mean square distance between occupied sites that belong to the same cluster, D is the fractal dimension of the cluster, and E is the Euclidean dimension where $E = 2$ is for a two-dimensional surface. According to Eq. (1), for length scale $L \ll \xi$, the largest cluster is self-similar and spans the whole box and $M(L) \sim L^D$; for $L \gg \xi$, the cluster looks homogeneous and $M(L) \sim L^E$. As shown in Fig. 2(d), the mass densities for the infinite cluster are scale dependent and follow the power law in Eq. (1) with $L \ll \xi$, and have the fractal dimension of $D = 1.71$.

The fractal dimension $D = 1.71$ of the infinite oxide cluster is inconsistent with the prediction by random percolation, which gives $D = 1.9$. The theory of random percolation deals with the formation of clusters by random occupation of sites, i.e., the probability of a site being occupied is independent of its neighbors. We speculate such a random site occupation mechanism does not apply to metal oxidation, where the oxide nuclei can act as capture centers to attract oxygen atoms for the oxide growth. This implies that the probability of site occupation is neighbor dependent for surface oxidation, and sites adjacent to the periphery of existing oxide have larger probability to be occupied.

We use KMC simulations to verify the above speculation. The basic processes in KMC simulations include random deposition of oxygen atoms onto a Cu surface and capture of the deposited oxygen atoms either by independent Cu surface sites (e.g., the process corresponding to nucleation of oxide islands) or by the surface sites adjacent to existing oxide islands (if any), leading to the oxide growth. The probability for oxygen atoms being captured by existing oxide islands is larger than the nucleation of new islands due to the smaller activation energy for an oxygen atom sticking to an existing oxide island. The formation of percolating oxide structure is observed from our KMC simulations and Fig. 3(a) shows the infinite cluster from simulations at the percolation threshold. Analysis of the mass densities of the infinite cluster reveals the power law of Eq. (1) and a fractal dimension of $D = 1.75$ with $L \ll \xi$ [Fig. 3(b)], which is very close to the fractal dimension ($D = 1.71$) of the infinite oxide cluster observed experimentally. Their agreement supports our speculation that the percolating oxide film growth during

Cu(111) oxidation is related to the processes of neighbor-dependent site occupation of oxygen.

One might expect that the mechanism of neighbor-dependent site occupation is typical for oxide growth during metal oxidation. This implies that percolating oxide film growth could be a general phenomenon for metal oxidation. However, our *in situ* TEM observations of the oxidation of Cu(100), Cu(110), and Cu(111) under similar oxidation conditions reveal that the oxidation of Cu(100) and (110) leads to the formation of 3D compact Cu_2O islands,[8–10,16,17] which obviously deviates from the fashion of percolating oxide growth. To address these seemingly contradictory oxidation behaviors on the different surface orientations, we start with consideration of the effect of oxygen surface chemisorption on oxide formation during metal oxidation. Many investigations have elegantly demonstrated that Cu(100), (110), and (111) surfaces show different reconstructions due to oxygen chemisorption. Oxidation of Cu(100) surfaces leads to the formation of an ordered $(\sqrt{2} \times 2\sqrt{2})R45°$ O–Cu(100) structure, where every fourth [100] row of the uppermost Cu atoms is missing (e.g., missing-row structure) with a corrugation of 0.35 Å.[18] The oxygen chemisorption on Cu(110) surface results in the formation of a (2×1)O–Cu(110) structure (added-row structure), where every second [100] row of the outermost Cu atoms is displaced outward by 0.8 Å.[19] The O chemisorption on Cu(111) results in ordered $29 - (\sqrt{13}R46.1° \times 7R21.8°)$ and $44 - (\sqrt{73}R5.8° \times \sqrt{21}R - 10.9°)$ lattice structures, which comprise distorted hexagonal arrays of O atoms with unit cell areas 29 and 44 times larger than that of the substrate Cu(111).[20–22] The oxygen atoms in the 29 and 44 structures have more than one well-defined height with corrugation up to $\sim$3.1 Å with respect to the Cu surface.[20,21,23] Compared to the chemisorbed structures of $(\sqrt{2} \times 2\sqrt{2})R45°$ O–Cu(100) and (2×1)O–Cu(110), the oxygen-chemisorbed '29' and '44' structures on Cu(111) surfaces have much larger surface corrugation, and such enhanced surface roughness can greatly inhibit surface diffusion of oxygen atoms. It has been widely observed and modeled that the morphologies of islands formed during thin film deposition closely depend on surface mobilities of adatoms, i.e., efficient surface and edge diffusions usually lead to compact island growth, while sluggish surface diffusion causes ramified island morphologies.[24,25] Our observations suggest these principles apply as well to the growth morphologies of oxide films during transient oxidation of metals. The percolating oxide growth during Cu(111) oxidation is related to the restricted surface diffusion of oxygen due to the highly corrugated O–Cu(111) surface structure, and the compact ox-ide island growth observed during the oxidation of O–Cu(100) and O–Cu(110) surfaces is related to the efficient oxygen surface diffusion due to their smooth surface structures.

In summary, we have observed percolating oxide growth during Cu(111) oxidation. The fractal dimension extracted from scaling analysis of the oxide films is consistent with a mechanism of neighbor-dependent site occupation of oxygen. The insights obtained from this study have broader implications to understanding transient oxidation of metals, where oxygen surface chemisorption generally occurs, but their effect on the oxide growth still remains poorly understood.

[1] C. Wagner, Z. Phys. Chem. **B21**, 25 (1933).
[2] W. W. Smeltzer, R. R. Haering, and J. S. Kirkaldy, Acta Metall. **9**, 880 (1961).
[3] J. Stringer, in *Point Defects and Transport in Oxides*, edited by M. S. Seltzer and R. J. Jaffee (Plenum, New York, 1974), pp. 495–517.
[4] J. Atkinson, Rev. Mod. Phys. **57**, 437 (1985).
[5] J. C. Yang, B. Kolasa, J. M. Gibson, and M. Yeadon, Appl. Phys. Lett. **73**, 2841 (1998).
[6] J. C. Yang, M. Yeadon, B. Kolasa, and J. M. Gibson, Appl. Phys. Lett. **70**, 3522 (1997).
[7] J. C. Yang, M. Yeadon, B. Kolasa, and J. M. Gibson, Scr. Mater. **38**, 1237 (1998).
[8] G. W. Zhou and J. C. Yang, Phys. Rev. Lett. **89**, 106101 (2002).
[9] G. W. Zhou and J. C. Yang, Appl. Surf. Sci. **210**, 165 (2003).
[10] G. W. Zhou and J. C. Yang, Appl. Surf. Sci. **222**, 357 (2004).
[11] M. L. McDonald, J. M. Gibson, and F. C. Unterwald, Rev. Sci. Instrum. **60**, 700 (1989).
[12] G. W. Zhou and J. C. Yang, Phys. Rev. Lett. **93**, 226101 (2004).
[13] A cluster is defined as a set of occupied sites all of which are connected by neighboring occupied sites. The connectivity checking algorithm in this study is developed based on examination of eight neighbors of each occupied pixel site. Any occupied sites on neighboring sites belong to the same cluster.
[14] J. Fender, *Fractals* (Plenum, New York, 1988).
[15] D. Stauffer, Phys. Rep. **54**, 1 (1979).
[16] G. W. Zhou and J. C. Yang, Surf. Sci. **531**, 359 (2003).
[17] G. W. Zhou, L. Wang, and J. C. Yang, J. Appl. Phys. **97**, 063509 (2005).
[18] F. Jensen, F. Besenbacher, E. Lagsgaard, and I. Stensgaard, Phys. Rev. B **42**, 9206 (1990).
[19] F. M. Chua, Y. Kuk, and P. J. Silverman, Phys. Rev. Lett. **63**, 386 (1989).
[20] F. Jensen, F. Besenbacher, E. Lagsgaard, and I. Stensgaard, Surf. Sci. **259**, L774 (1991).
[21] F. Jensen, F. Besenbacher, and I. Stensgaard, Surf. Sci. **269–270**, 400 (1992).
[22] T. Matsumoto, R. A. Bennett, P. Stone, T. Yamada, K. Domen, and M. Bowker, Surf. Sci. **471**, 225 (2001).
[23] S. M. Johnston, A. Mulligan, V. Dhanak, and M. Kadodwala, Surf. Sci. **519**, 57 (2002).
[24] M. Z. Li and J. W. Evans, Phys. Rev. B **69**, 035410 (2004).
[25] R. Q. Hwang, J. Schroder, C. Gunther, and R. J. Behm, Phys. Rev. Lett. **67**, 3279 (1991).